Energy 138 (2017) 1–9

Contents lists available at ScienceDirect

Energy

journal homepage: www.elsevier.com/locate/energy

# Analytic modeling of parabolic trough solar thermal power plants

Germán A. Salazar [a, b], Naum Fraidenraich [a], Carlos Antonio Alves de Oliveira [c], Olga de Castro Vilela [a], Marcos Hongn [b], Jeffrey M. Gordon [d, *]

[a] Departamento de Energia Nuclear, Grupo de Pesquisas em Fontes Alternativas de Energia, Universidade Federal de Pernambuco, Av. Prof. Luiz Freire, 1000-DCU, CEP 50740-540, Recife, PE, Brazil
[b] Instituto de Investigaciones en Energias No Convencionales, Av. Bolivia 5150, A4408FVY, Salta, Argentina
[c] Instituto Federal de Alagoas, Campus Palmeira dos Índios, Av. Alagoas, Palmeira de Fora, 57608-180, Palmeira dos Índios, AL, Brazil
[d] Department of Solar Energy and Environmental Physics, Blaustein Institutes for Desert Research, Ben-Gurion University of the Negev, Sede Boqer Campus, 84990, Israel

ARTICLE INFO

*Article history:*
Received 31 March 2017
Received in revised form
5 July 2017
Accepted 17 July 2017
Available online 18 July 2017

*Keywords:*
Analytic modeling
Parabolic troughs
Solar thermal
Solar power
Transients

ABSTRACT

We derive, evaluate and validate comprehensive analytic modeling of the energy flows in parabolic trough solar thermal power plants. The analytic formulae are straightforward to implement and evaluate, relating to the heat transfer within and from the solar concentrators (including transients, mainly overnight heat losses), and the impact of solar field operation on turbine power and efficiency. Prior numerical simulations used to design solar thermal power systems have either been proprietary or devoid of a fully-reported source code - hence inaccessible or problematic for widespread use. Also, the dependence of these simulations on extensive numerical procedures does not provide a transparent physical picture that grants a clear understanding of how component and system performance vary with the principal operating and input variables - a drawback overcome by the analytic approach presented here. Published experimental measurements of sufficient extent to permit meaningful comparisons between theory and experiment for such solar thermal power plants are exceptionally limited. This narrow data base is used for model validation on both a monthly and an hourly basis. The analytic model is then applied to evaluating a solar power plant now being planned for northeast Brazil, also highlighting the energy-delivery advantages of low-latitude locations.



## 1. Introduction

Of the roughly 5 GW of operational commercial solar thermal power plants, about 85% comprise single-axis-tracking parabolic trough concentrators driving steam turbines [1] (Fig. 1). Almost all systems use an oil coolant pumped through (a) evacuated receiver tubes at a variable flow rate that maintains a fixed collector outlet temperature, followed by (b) a heat exchanger the secondary of which feeds the power block. Gas-fired backup operates in parallel with solar so as to ensure the turbine receives a prescribed constant flow rate of fixed-temperature steam, thereby achieving uninterrupted electricity production independent of solar intermittency. The overwhelming majority of these installations do not employ thermal storage [1,2].

Systems installed to date have been designed with large-scale numerical computer simulations that compute all energy flows as a function of the meteorological and operating variables. Most of these simulations are proprietary or lacking a full source code - hence problematic to implement [2]. Other simulations are based on cumbersome encoded and unalterable numerical procedures that preclude a clear physical understanding of how each facet of system performance varies with the input and operational variables [3–8]. Moreover, in addition to their complexity, most available simulations are rather focused on specific systems.

Ongoing research in this area covers the modeling, design and evaluation of system components - as well as overall system performance assessments - performed with the types of complex numerical procedures noted above. Recent papers have addressed pivotal issues that include (1) collector and turbine properties, sizing, and control strategies [9–14], (2) how short-term and long-term solar availability affects system yield [15], (3) the influence of thermal storage [14,15], and even (4) how artificial neural networks can facilitate system design and evaluation [16].

* Corresponding author.
*E-mail address:* jeff@bgu.ac.il (J.M. Gordon).

http://dx.doi.org/10.1016/j.energy.2017.07.110
0360-5442/

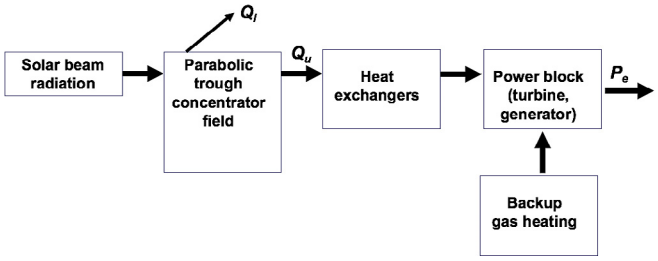


**Fig. 1.** Schematic energy flow diagram for a solar thermal power plant generating AC electrical power $P_e$, with parallel gas-fired backup ensuring a specified steam flow rate to the turbine. $Q_u$ is useful thermal power delivery. $Q_l$ is heat loss to ambient. $P_e$ is net electricity generation.

Comparing model predictions against field performance turns out to have considerable limitations. *Published* experimental measurements of both solar beam irradiance and detailed solar thermal power plant performance (including separate monitoring of the collector field and the turbine block) appear to be surprisingly uncommon. To our knowledge, verifiable monthly-average figures for all required measurements are restricted to a single year. Additionally, hour-by-hour data are limited to a single clear day. Both come from one particular large-scale installation in Kramer Junction, CA, US [2,17]. These data provide the basis for our comparisons of theory versus experiment.

As for analytic modeling of system performance, a first step was taken in Ref. [18], but (a) did not relate to transients (most notably collector nighttime cool-down losses), (b) did not account for the sizable gap between instantaneous and long-term performance, and (c) did not accommodate different collector flow strategies.

In overcoming these limitations, the analytic model developed here (1) offers physical transparency for the main processes impacting collector and turbine performance (as opposed to the modeling being tacitly embedded within complicated numerical simulation procedures, *vide infra*), (2) can readily be applied to a variety of solar thermal power systems, and (3) is amenable to evaluation by any user via straightforward calculations.

The rest of the paper is organized as follows. Section 2 presents the general method with full details on collector, system and turbine modeling. This includes modeling the optical and thermal energy flows of the solar collector field, how the state of the steam produced by the solar field impacts turbine performance, and collector nighttime cool-down losses. Section 3 comprises the results and discussion: a case study with comparisons of theory vs. experiment for both solar collector efficiency and overall system electrical efficiency, plus the design of a solar thermal power plant currently being planned. Section 4 summarizes our conclusions, emphasizing the new added value of the analytic modeling for analyzing and designing solar thermal power plants.

## 2. General method and modeling

### 2.1. Modeling collector optical gains

The solar power absorbed by the collectors per absorber area, $Q_{abs}$, is

$$Q_{abs} = I_{bn} \cos(\theta)\, FS\, K(\theta)\, \eta_o\, C_g \;=\; I_{coll}\; C_g \tag{1}$$

where $I_{bn}$ is the incident *normal* solar beam irradiance (per aperture area), $\theta$ is the solar incidence angle on the aperture [19], $FS$ is the unshaded fraction of collector aperture (a function of solar geometry and field layout, for which the closed-form expression is presented in Ref. [20]), and $I_{coll}$ denotes the *collected* solar irradiance per aperture area. In contrast, "collectible" radiation refers just to the product $I_{bn}\cos(\theta)$, which is the solar beam irradiance incident on the aperture. Geometric concentration ratio $C_g$ is typically ~20–25 (defined as the ratio of collector aperture area $A_{coll}$ to absorber area $A_{abs}$, with $A_{abs}$ relating to absorber tube circumference $W$ times its length $L$). $\eta_o$ is the collector optical efficiency at normal incidence, comprising the product of mirror reflectivity, receiver tube transmittance, receiver coating absorptance, and receiver intercept factor [19]. $K(\theta)$ is the incidence angle modifier [19], which measures how optical gains vary with $\theta$ relative to their value at normal incidence ($K(0) \equiv 1$). $K(\theta)$ subsumes how the transmission of the glazing, the absorption of the absorber coating, and the width of the sun's image projected onto the receiver tube by the concentrator vary with incidence angle.

### 2.2. Modeling collector heat transfer

The instantaneous useful thermal power delivery per unit length (in W/m), as a function of position $x$ along the collectors, $Q_u(x)$ ($0 \le x \le L$ from entry to exit) is proportional to the difference between the local absorber temperature $T_{abs}(x)$ and fluid temperature $T_f(x)$:

$$Q_u(x) = Wh\Big(T_{abs}(x) - T_f(x)\Big). \tag{2a}$$

The convective heat transfer coefficient $h$ between the coolant and the absorber can be obtained from the dimensionless Nusselt number $Nu$

$$h = \frac{k}{D_i} Nu \tag{2b}$$

where $k$ is the thermal conductivity of the fluid, and $D_i$ is the internal diameter of the absorber tube ($D_i = 0.066$ m for the example considered here, with the tube outer diameter being 0.070 m). For fully-developed turbulent flow (the dimensionless Reynolds number $Re > 10{,}000$) in long tubes (length/diameter > 60), and for the dimensionless Prandtl number Pr in the range $0.7 < Pr < 160$, $Nu$ is given by the Dittus-Boelter correlation [21].

$$Nu = 0.023 Pr^{0.4} Re^{0.8}. \tag{2c}$$

$\mathrm{Pr} = \nu/\alpha = \mu/(\rho\,\alpha)$, where $\nu$ is the kinematic viscosity of the fluid, $\mu$ is the dynamic viscosity, and $\rho$ is the density. $\alpha$ is the thermal diffusivity $\alpha = k/(\rho\, C_p)$ where $C_p$ is the specific heat of the fluid. $\mathrm{Re} = v\, D_i/\nu$, where $v$ is the linear flow velocity. For example, during solar power generation, and for the physical properties of the collector fluid [22], one obtains $\mathrm{Pr} = 5.5$ and $\mathrm{Re} = 4.0\cdot 10^5$, yielding $h = 1.8\cdot 10^3$ W/(K-m$^2_{\text{inner tube}}$). In all our equations for collector energy balance, $h$ is expressed per unit area of *outer* tube, i.e., modified by the ratio of tube inner-to-outer area, $(0.066/0.070)^2 = 0.889$.

Equation (2) relates to heat transfer *within* the collector. For heat transfer *from* the collector *to* the environment, we base the analysis on experimental measurements from the evacuated selectively-coated receiver tube considered here [23]. The data reported in Ref. [23] also included measurements for non-evacuated, air-filled, and unglazed receiver tubes, as well as for a different selective coating, but the relevant results here are those pertaining to the receiver tubes installed in the solar field for which system performance data were available.

A simulation model for evaluating the heat losses for several configurations of glazed receiver tubes was derived in Ref. [8]. The results were empirically correlated as third-order polynomials in the average temperature of the collector coolant [24], and

compared favorably against the earlier experimental measurements in Ref. [23].

The value of computational models and best-fit non-linear regressions notwithstanding - and given that [23] reports the measured heat losses for the exact same evacuated receiver tube installed in the SEGS VI solar power system analyzed below - we chose to base our analysis on data, and found the heat loss measurements to be well approximated by a quadratic function of the temperature difference between the local absorber temperature and the environmental temperature $\Delta T = T_{abs}(x) - T_e$. Specifically, the rate of absorber heat loss per unit length $Q_l$ is well approximated by:

$$Q_l = W\left(U_o \Delta T + U_1 (\Delta T)^2\right) \tag{3}$$

with thermal loss coefficients $U_o$ and $U_1$, and with which one can define a collector temperature-dependent heat loss coefficient $U$ (in W/(K-m$^2_{abs}$)):

$$U = \frac{1}{W}\frac{dQ_l}{d(\Delta T)}. \tag{4}$$

$Q_u(x)$ (Eq. (2a)) can also be expressed as

$$Q_u(x) = \dot{m}_f C_p \frac{dT_f(x)}{dx} \tag{5}$$

where $\dot{m}_f$ is the coolant mass flow rate and $C_p$ its specific heat. In differential form, Eqs. (2a) and (5) can be recast as

$$\frac{dQ_u(x)}{dx} = -\left[\frac{1}{\frac{1}{h}+\frac{1}{U}}\right]\left[\frac{W}{\dot{m}_f C_p}\right] Q_u(x). \tag{6}$$

The differential Eq. (6) can be integrated to obtain the implicit closed-form solution for $x$ as a function of $Q_u$ ($x = x(Q_u)$). Then, evaluating the solution at the collector exit ($x = L$) yields

$$\dot{m}_f C_p = -\frac{W\,L}{\frac{1}{h} ln\left(\frac{Q_u(L)}{Q_u(0)}\right) + \frac{1}{U_s} ln\left(\frac{\left(U_s - \left(U_s^2 - 4U_1 Q_u(L)\right)^{0.5}\right)\left(U_s + \left(U_s^2 - 4U_1 Q_u(0)\right)^{0.5}\right)}{\left(U_s + \left(U_s^2 - 4U_1 Q_u(L)\right)^{0.5}\right)\left(U_s - \left(U_s^2 - 4U_1 Q_u(0)\right)^{0.5}\right)}\right)}. \tag{7}$$

The function $U_s$ in Eq. (7) is equal to $[U_o^2 + 4U_1 Q_{abs}]^{0.5}$, where $Q_{abs} = (Q_u(x) + Q_l(x))/W$ is treated as independent of $x$.

The useful solar thermal power delivery from the full solar field $Q_u$ (in W) is then

$$Q_u = \int_0^L Q_u(x)\,dx = \dot{m}_f C_p (T_4 - T_1). \tag{8}$$

We emphasize that the collector flow rate is expressed exclusively as a function of $Q_{abs}$ (recall that $U_s$ in Eq. (7) is a known function of $Q_{abs}$), which in turn has an explicit dependence on the instantaneous solar beam irradiance and on the environmental temperature $T_e$.

The collector inlet fluid temperature $T_f(x = 0) = T_1$ is established by the heat exchange process being optimized for maximum efficiency of the solar thermal power plant [18]. The collector outlet fluid temperature $T_f$ ($x$=$L$) = $T_4$ is ordained by its maximum safe operating temperature of 391 °C [22], at least for the oil used in most solar thermal power plants to date [1,2].

The absorber temperature at the collector inlet and outlet can now be evaluated (details in Ref. [25])

$$\begin{aligned} T_{abs}(0) &= T_e + \left(\frac{h+U_o}{2U_1}\right)\left(-1 + \left(1 + \left(\frac{4U_1(Q_{abs} + h(T_1 - T_e))}{(h+U_o)^2}\right)\right)^{0.5}\right) \\ T_{abs}(L) &= T_e + \left(\frac{h+U_o}{2U_1}\right)\left(-1 + \left(1 + \left(\frac{4U_1(Q_{abs} + h(T_4 - T_e))}{(h+U_o)^2}\right)\right)^{0.5}\right) \end{aligned}. \tag{9}$$

Using Eq. (2a) to solve for $Q_u$ at the collector entry ($x = 0$) and exit ($x = L$) provides an analytic expression for the collector thermal flow rate $\dot{m}_f C_p$ (Eq. (7)).

The collectors are operated such that their fluid thermal flow rate follows variations in solar radiation so as to maintain constant pre-determined values of $T_1$ and $T_4$, independent of solar irradiance (Eq. (7)), provided that irradiance exceeds the collector's turn-on threshold. The threshold refers to the minimum value of collectible radiation at which the prescribed collector operating outlet temperature for power generation can be attained.

In reality, steam generation does not end *exactly* when $T_4$ is not reached. The combination of standard governing feedback controls and a solar field response time of the order of minutes under flow (operating) conditions [6,26] stabilize these transitions, while ensuring that deviations of $T_1$ and $T_4$ from their pre-set values are small.

### 2.3. Modeling collector transients and cool-down losses

The analyses portrayed above relate to steady-state conditions. Solar beam radiation data are most commonly available only on an

hourly time scale (rather than, for example, a 1-min basis). How large an error accrues due to an hour-by-hour steady-state analysis, as opposed to a rigorous dynamic or transient solution? Independent of the answer, there are also transient overnight cool-down losses every day, which must be evaluated and, as we'll see below, are non-negligible and can be expressed analytically.

For a given hour or day fraught with interruptions due to scattered clouds, the difference in energy delivery between a proper transient analysis and the steady-state approximation can be non-negligible [6,7,26,27]. However, for climates with high direct radiation (hence suitable for solar concentrator power plants), the error in annual solar energy delivery is less than 1% [27], and hence not pursued further here. Rather, we focus on deriving the contribution of nighttime cool-down losses.

Of the assortment of operating strategies proposed for nighttime management of the collectors, the most commonly adopted one - analyzed here - is permitting the collector coolant to cool, but heating it (via a heat exchanger) by gas combustion at system start-up each morning [2].

With no solar input, and hence no collector flow, the average temperature of the collector coolant $T_f$ varies with time $\tau$ as

$$\frac{dT_f}{d\tau} = -\frac{L\,Q_l}{C_p\,\rho\,V} \tag{10}$$

where $V$ denotes the coolant volume in the absorber tubes. $Q_l$ can be expressed a function of the difference between $T_f$ and the temperature of the absorber's external wall $T_{abs,ext}$

$$Q_l = W\frac{T_f - T_{abs,ext}}{\frac{1}{h} + \frac{t_{wall}}{k_{wall}}} \tag{11}$$

where $1/h$ is the thermal resistance from the coolant to the absorber wall. $t_{wall}$ and $k_{wall}$ are the thickness and thermal conductivity of the absorber tube wall, respectively. With $t_{wall} = 0.002$ m and $k_{wall} = 55$ W/(m-K) for the example considered here, $1/h \gg t_{wall}/k_{wall}$. During the nighttime no-flow period, $1/h$ is approximated as the thermal resistance across a stagnant fluid layer: $1/h = D_i/(2k)$.

Equating thermal power losses in Eqs. (3) and (11), and writing $T_f$ - $T_{abs,ext}$ as ($T_f$ - $T_e$) - ($T_{abs,ext}$ - $T_e$) in Eq. (11), the second-order equation in ($T_{abs,ext}$ - $T_e$) can be expressed in terms of $T_f$ - $T_e$

$$T_{abs,ext} - T_e = \frac{U_o + h}{2\,U_1}\left[-1 + \sqrt{1 + \frac{4\left(T_f - T_e\right)U_1\,h}{(U_o + h)^2}}\right]. \tag{12}$$

A proper solution for $T_f(\tau)$ requires accounting for the temperature dependence of $\rho$, $C_p$ and $k$, based on the physical properties of Terminol VP-1, which are reported in Ref. [22]. Inserting Eqs. (11 and 12) and the coolant's physical properties [22] into Eq. (10) yields a first-order differential equation that can be solved for $T_f(\tau)$.

### 2.4. Additional control issues

Another consideration is how to handle the surplus when the thermal power from the solar field exceeds the power block's capacity. Here, we model that excess energy as dumped to the environment (via any convenient control). It should be noted, however, that alternative strategies include (a) allowing the turbine to operate above its rated capacity, or reducing its temperature by bypassing the feedwater heater [2], and (b) partial defocusing of all collectors or total defocusing of some collectors [7].

An additional system energy loss is the parasitic energy for pumping coolant through the collector field. This represents a case-specific variable that is not modeled here - further complicated by parasitics depending not only on the fraction of daytime steam generation provided by gas backup, but also by whether coolant is circulated through the collectors not only when collectible radiation is available, but 24 h a day in order to lessen the danger of thermal shocks to the evacuated receiver tubes and the pumps [2]. We note, however, that parasitics in the installed solar thermal power plants for which published data are available [2,28] was ~12% of the electrical energy generation. To wit, with a yearly-average system conversion efficiency of ~14% [2,28], parasitics represented ~1.7% of the yearly collectible solar radiation.

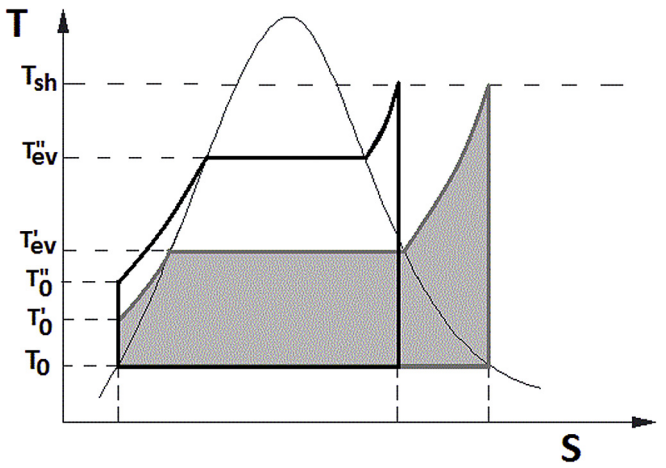


**Fig. 2.** Temperature-entropy ($T$–$S$) diagram for two Rankine cycles (shaded with thick gray curves, and unshaded with thick black curves) constrained to have the same superheated steam temperature at the turbine entry, but with different evaporation temperatures. The thin black line indicates water's coexistence curve.

### 2.5. Turbine modeling

The aim is to explicitly provide the full scope of analytic methods used here for modeling the power block, with no presumption of this section introducing new observations. The Rankine cycle turbine must be optimized with respect to the evaporation temperature $T_{ev}$ and the turbine inlet superheated vapor pressure $p_{sh}$, subject to a given value of superheated steam temperature $T_{sh}$. This is illustrated in the temperature-entropy ($T$-$S$) diagram of Fig. 2, for two Rankine cycles constrained to have the same superheated steam temperature at the turbine entry, but with different evaporation temperatures $T_{ev}$ (primed and double-primed) and corresponding pressures. The condensed water pressure $p_o$ at temperature $T_o$ is increased to pressure $p_o'$ or $p_o''$ and temperature $T_o'$ or $T_o''$, respectively, by a pump at the condenser outlet. The pressure at the turbine inlet $p_{sh}$ is $p_o'$ or $p_o''$, corresponding to $T_{ev}'$ or $T_{ev}''$.

The delivered electrical power depends on the type of Rankine cycle and its isentropic efficiency. The examples below are based on: (a) a standard Rankine cycle in which there is no regeneration, (b) a constant isentropic efficiency, and (c) negligible heat losses in the heat exchanger.

The analytic energy balance equations for evaluating turbine performance have been summarized in Refs. [20,29,30]. They apply equally well here, and, for economy of presentation, are not reiterated. The turbine mechanical work is equal to the enthalpy difference between the states at temperatures $T_{sh}$ and $T_o$' or $T_o$" in the $T$-$S$ diagram shown in Fig. 2, and thereby depends on $T_{ev}$.

## 3. Results and discussion: a case study

### 3.1. Collector and turbine characteristics

Despite thousands of MW of installed solar thermal power systems, published performance data are scarce. Particularly prominent are the records for the thermal and electrical efficiencies measured at the Kramer Junction, CA plant (latitude 35°N, with an annual normal solar beam irradiance of 2.725 MWh/m$^2$) [17]) [28], specifically the SEGS VI system, installed in 1989, designed for a peak electrical power delivery of 30 MW, with a measured annual electrical conversion efficiency of 0.14, defined as annual AC electrical energy generation relative to annual collectible solar beam radiation. The solar field comprises 188,000 m$^2$ of Luz Corp. LS-2 parabolic trough concentrators, with Solel UVAC evacuated selectively-coated receivers at their focus (Table 1). The collector heat transfer fluid is Therminol oil (see Ref. [22] for its thermophysical properties). The field is operated such that the oil temperature is 390 °C at the collector field outlet during solar power generation. The corresponding collector turn-on/off threshold is ~120 W/m$^2$.

The steam turbine has a net capacity of 30.0 MW (at a gross capacity of 35.0 MW), operating at a pressure of 100.0 bar, with a full-load turbine efficiency of 0.375 and natural-gas heating backup to supplement solar input as required. Turbine block characteristics are listed in Table 2. The dependence of turbine thermal-to-mechanical efficiency on $T_{ev}$ is plotted in Fig. 3. Turbine temperatures $T_{ev}$ and $T_{sh}$ are typically chosen for maximum power production (i.e., maximum work per cycle). In this example, the maximum-work point $T_{ev}$ = 310 °C was chosen, for which the turbine efficiency is 0.39.

### 3.2. Comparing analytic model predictions against field measurements

The only extensive data sets published appear to be month-by-month efficiency results [28]. A complete one-year data set - along with the corresponding predictions of the analytic model - are summarized in Fig. 4. Collector efficiency is defined as the ratio of the monthly energy delivered by the solar field (hourly $Q_u$ summed over a given month) to the total *collectible* solar beam radiation (hourly $I_{bn}\cos(\theta)$ summed over the same month). The solar delivery $Q_u$ includes losses due to optical efficiency, incidence-angle modifier and collector heat losses. Overall system electrical efficiency is defined as the total net AC electrical energy delivered $P_e$, relative to the total collectible solar beam radiation during that same period. The RMS differences between the data and the analytic predictions are 4.0% (absolute) for collector efficiency, and 1.0% (absolute) for overall system electrical efficiency. For comparison, computations of the latter (i.e., of month-by-month overall system electrical efficiency) using a state-of-the-art computer simulation for this system yielded an RMS difference of 0.7% (absolute) between measurements and simulated performance [2].

There was only a single day - near summer solstice, at the Kramer Junction system [28] - with a complete published (but unannotated) hour-by-hour data set, against which we could compare model predictions on this far shorter time scale (Fig. 5).

**Table 2**
Power block parameters.

| Power block characteristic | Value |
|---|---|
| Steam condensation temperature | 40 °C |
| Evaporation temperature $T_{ev}$ | 310 °C |
| Superheating temperature $T_{sh}$ | 371 °C |
| Turbine isentropic efficiency | 0.80 |
| Governing performance equations | [20,29,30] |
| Generator efficiency | 0.97 |

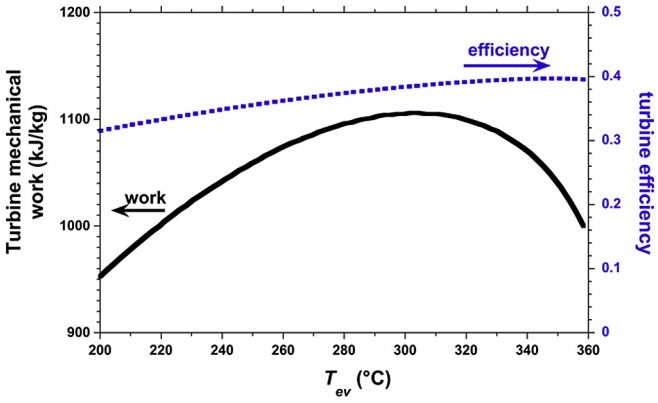


**Fig. 3.** Turbine mechanical work and turbine thermal-to-mechanical efficiency as a function of $T_{ev}$.

**Table 1**
Solar concentrator properties [23].

| Solar concentrator characteristic | Value |
|---|---|
| Collector optical efficiency at normal incidence $\eta_o$ | 0.733 |
| Concentrator mirror aperture (width) | 5.0 m |
| Geometric concentration ratio $C_g$ | 22.74 (absorber tube outer diameter = 0.07 m) |
| Concentrator length L | 47.1 m |
| Number of collectors per row | 8 |
| Number of collector rows | 100 (Kramer Junction)<br>5 (Petrolina) |
| Total concentrator aperture area | 188,400 m$^2$ (Kramer Junction)<br>9420 m$^2$ (Petrolina) |
| Collector inlet fluid temperature | 308 °C |
| Collector outlet fluid temperature | 391 °C |
| Single-axis tracking mode | North-south horizontal[a] |
| Incidence angle modifier, $K(\theta)$ | $K(\theta) = \cos(\theta) + 0.02012\ \theta - 0.01030\ \theta^2$ ($\theta$ in rad) |
| Collector heat-loss coefficient, $U_o + U_1(T_{abs} - T_e)$ | $U_o = -0.2556$ W/(K-m$^2_{abs}$)<br>$U_1 = 0.01817$ W(K$^2$-m$^2_{abs}$) |

[a] Basically all parabolic-trough solar thermal power plants use one-axis north-south (N-S) horizontal tracking. Among horizontal-axis azimuths, N-S maximizes yearly collectible radiation [19]. For summer-peaked electricity demand, N-S has the added advantage of a summer-averaged cos(θ) close to unity. Also, as latitude grows smaller, N-S horizontal approaches polar-axis tracking, which reaches 97% of the collectible radiation of two-axis tracking [19].

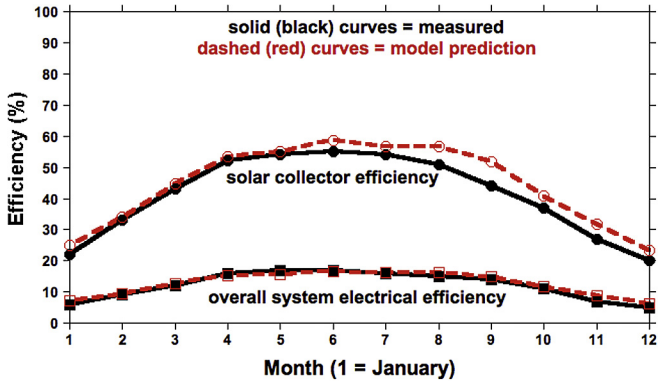


**Fig. 4.** Month-by-month measured and predicted solar collector efficiency and overall electrical system efficiencies in Kramer Junction, CA.

Two extenuating circumstances should be considered here. First, no explanation was provided in the field measurement record as to why there appears to be an approximately 1-h delay in starting the gas heating of the collector fluid. Second, no explanation was provided regarding why there was more than a 1-h delay in starting the operation of the turbine block, namely, why electricity generation was only started more than 1 h after the collectors were already providing a sufficient quality and flow of steam to drive the turbine. In addition, no comments were provided about why solar collector efficiency exhibited a non-negligible dip around noon, despite the constancy of the solar beam radiation *and* despite the measured overall system electrical efficiency remaining constant over the same period.

These ambiguities may be partly related to the fact that the control strategies implemented by the plant operators were not reported, and hence cannot be reproduced in the computations. For example, as can be seen in Fig. 5, sharp variations in collector efficiency occurred at the beginning and end of the collection period. This behavior does not follow the solar radiation. Although automated computerized systems were used in later solar thermal power plants in Kramer Junction [31], there is no detailed comprehensive published performance information available.

Such short-term uncertainties have a noticeably smaller impact on monthly-averaged performance than on hour-by-hour performance. Hence, although the differences between experiment and theory may be satisfactory for monthly-integrated performance, there can be more substantial discrepancies for a particular day on an hourly basis. This is one possible contributing factor to the differing degree of agreement between theory and experiment in Fig. 4 (month-by-month data) and 5 (hour-by-hour data).

### 3.3. Analytic design calculations for a solar thermal power plant in Petrolina, Brazil

In this section, the analytic model is used to estimate component and system performance for a pilot solar thermal power plant that is currently being planned for Petrolina, Brazil - a location with lower solar beam radiation than Kramer Junction, but at a far lower latitude (9.35°S), which bodes well for lower solar-geometry-related losses (mainly via a higher averaged $\cos(\theta)$ and $K(\theta)$). The collector and turbine parameters were taken to be the same as in Tables 1 and 2.

Extensive meteorological data were available from the local weather station [32], with complete uninterrupted data sets for the years 2011 and 2013, for which the calculations were performed. With the first pilot installation being planned for a peak electricity generation of 1.5 MW, the collector area chosen is about 20 times smaller than that for the Kramer Junction 30 MW plant (see Table 1).

Results of the analytic model computations for monthly and yearly performance are itemized in Table 3. The efficiencies (percentages) listed in the row summarizing annual total energy are the ratio of annual energy delivery to yearly collectible radiation. As expected from sun-earth geometry for the one-axis north-south horizontal tracking mode [19], the cosine effect for collectible radiation is more prominent around winter solstice (with Petrolina being in the *southern* hemisphere, winter solstice is on 21 June) than summer solstice (21 December).

### 3.4. Overnight collector cool-down losses

Sample results for the overnight collector cool-down dynamics derived in Section 2.3 are plotted in Figs. 6–7 for a representative high-irradiance day in Petrolina, Brazil [32]. The overnight cool-down period is about 12 h, during which the average coolant temperature decreases by 252 °C.

Because there is coolant flow during the gas-heating period, the

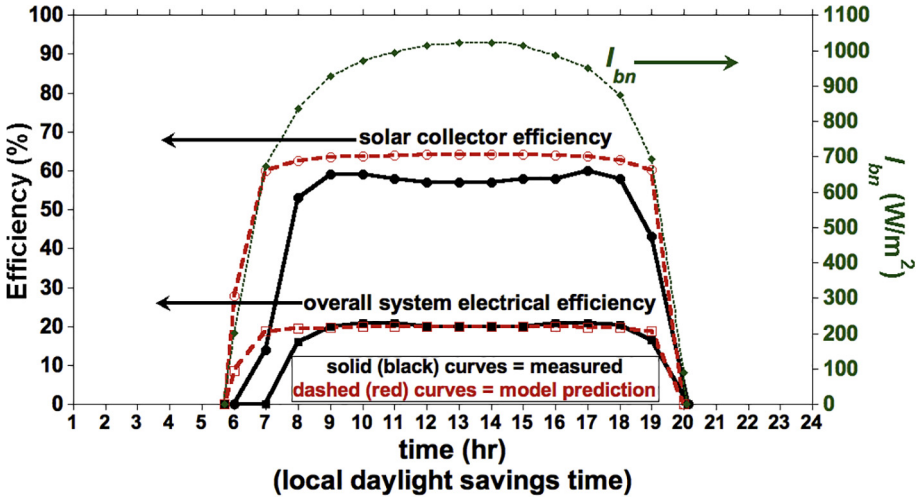


**Fig. 5.** Hour-by-hour measurements [28] of solar collector efficiency and overall system electrical efficiency, and the corresponding predictions of the analytic model, for a clear day near summer solstice at the solar thermal power system in Kramer Junction, CA. Measured normal solar beam irradiance is also shown.

**Table 3**
Monthly and annual performance computed with the analytic model, for the planned Petrolina plant. $A_{coll} = 9420$ m$^2$.

| Month | $I_{bn}$•$A_{coll}$ (MWh/day) | $I_{bn}$•$A_{coll}$•cos(θ) (MWh/day) | $Q_{abs}$•$A_{abs}$ (MWh/day) | $Q_u$ (MWh/day) | $P_e$ (MWh/day) |
|---|---|---|---|---|---|
| January | 40.45 | 39.16 | 26.77 | 19.92 | 5.69 |
| February | 34.78 | 34.48 | 24.40 | 17.74 | 5.03 |
| March | 41.39 | 41.15 | 28.94 | 21.69 | 6.18 |
| April | 37.50 | 36.12 | 24.20 | 17.35 | 4.91 |
| May | 26.98 | 24.33 | 15.00 | 9.40 | 2.64 |
| June | 41.19 | 35.73 | 21.34 | 14.91 | 4.24 |
| July | 40.26 | 35.48 | 21.66 | 14.98 | 4.25 |
| August | 59.52 | 55.68 | 36.19 | 28.37 | 8.15 |
| September | 56.34 | 55.52 | 38.33 | 30.76 | 8.82 |
| October | 54.54 | 54.34 | 38.17 | 30.44 | 8.72 |
| November | 48.75 | 47.57 | 33.04 | 25.72 | 7.38 |
| December | 52.69 | 50.56 | 34.53 | 26.85 | 7.71 |
| Annual avg. (MWh/day) | 44.53 | 42.51 | 28.55 | 21.51 | 6.14 |
| Annual total (MWh/year) | 16,278 | 15,535 | 10,429 (67.1%) | 7859 (50.5%) | 2244 (14.4%) |

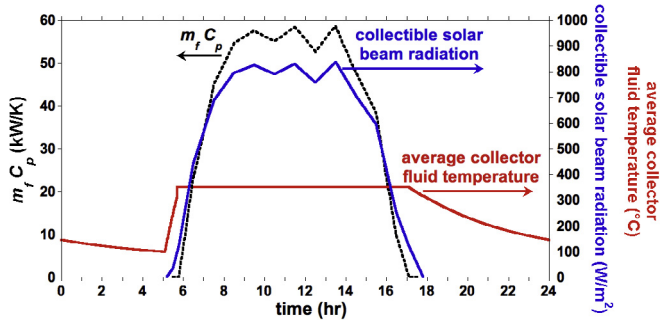


**Fig. 6.** Calculated collector flow $m_f C_p$ on the left-hand ordinate and calculated average fluid temperature on the right-hand ordinate along with the measured collectible solar beam irradiance, for a typical high-irradiance day in Petrolina, Brazil [32].

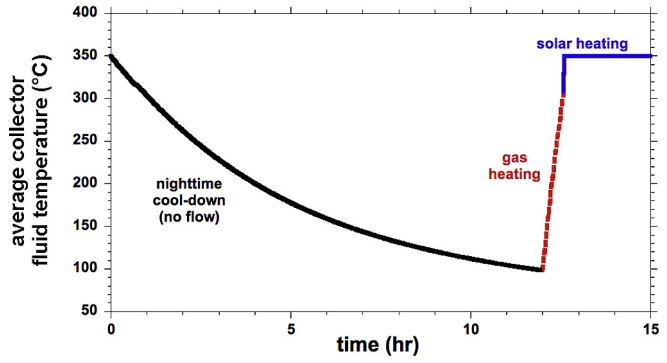


**Fig. 7.** Calculated average collector fluid temperature during overnight cooling and during morning gas-fired activation - a magnification from Fig. 6, but with time zero taken around sunset when the collector pump is turned off.

heat-transfer coefficient $h$ between the coolant and the tube's inner wall is dominated by forced convection. We conservatively adopted $h = 100$ W/(K-m$^2$), which is far higher than the corresponding $h$ during the no-flow cool-down period. Then from Eq. (10) - and even accounting for the temperature dependence of $h$ under forced convection - to a good approximation, $T_{abs,ext}$ approaches $T_f$ plus a small first-order correction in $1/h$.

Gas combustion is timed such that the average fluid temperature reaches its operational inlet value $T_1$ of 308 °C around the same time that the collectible radiation reaches its turn-on threshold value of ~120 W/m$^2$. The gas heater is then disengaged, and solar heating rapidly raises the coolant average fluid temperature to 350 °C (with the collector outlet temperature $T_4$ being raised to 391 °C) for the resumption of solar steam generation (Figs. 6–7).

The solution for the time evolution of $T_f$ requires modification of Eq. (10) to include the constant rate of gas heating ($H$, in W)

$$\frac{dT_f}{d\tau} = \frac{H - Q_l L}{C_p\, \rho\, V}. \tag{13}$$

One can either fix the heat-up time and obtain the gas heating thermal power needed, or input the thermal power and calculate the associated heat-up time. In the example here for Petrolina, we opted for a fixed gas-heating thermal power of 1.25 MW, for which the heat-up time (from 98 °C to $T_1 = 308$ °C) turns out to be 2130 s.

In Figs. 6–7, gas-fired heating of the collector coolant is activated slightly after 5 a.m., and timed so that, slightly more than half an hour after activation, the minimum temperature needed for steam generation coincides with solar beam irradiance reaching its nominal turn-on threshold. (In the absence of gas heating, the collector no-flow transient would result in collector flow only starting slightly after 8 a.m., with a concomitant loss of collectible radiation that exceeds the gas consumption - not indicated here for clarity of presentation.)

For a gas burner efficiency of 80%, the gas calorific value consumed is then 3.33 GJ, which is 4.3% of the yearly-average daily absorbed solar power $Q_{abs}$•$A_{abs}$ of 77.4 GJ (Table 3). Namely, nighttime cool-down losses are small, but non-negligible.

Thermal relaxation time is commonly defined as the period for the difference $\Delta T$ between the absorber temperature and the environmental temperature to decrease to $1/e \approx 0.37$ of its initial value (predicated on an approximately exponential decay of $\Delta T$

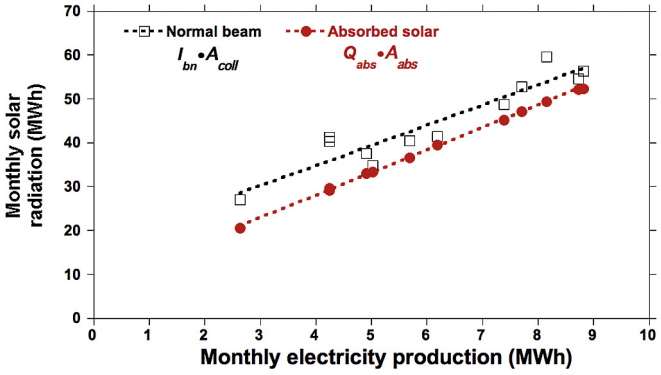


**Fig. 8.** The correlation of monthly electricity delivery with (a) monthly normal-beam radiation, and (b) monthly absorbed solar radiation as computed with the analytic model.

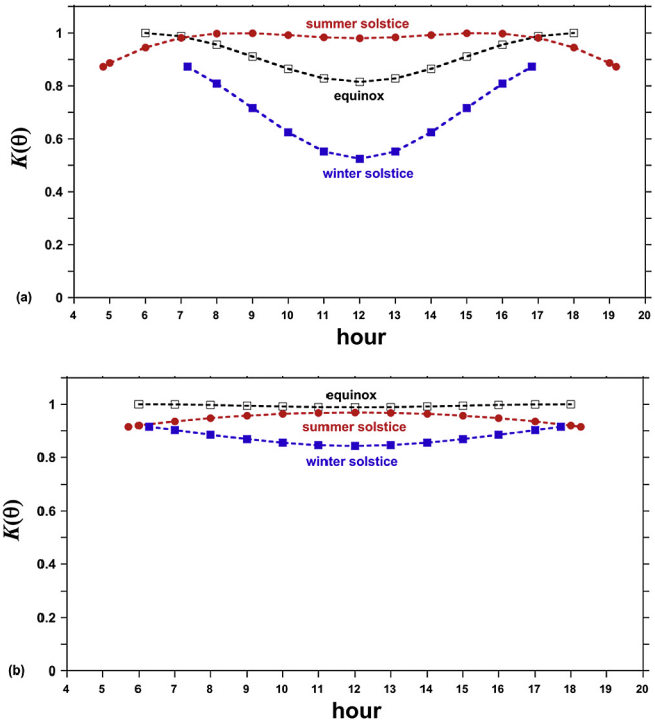


**Fig. 9.** Hourly incidence angle modifier $K(\theta)$ for representative days of high collectible radiation at the solstices and equinoxes. (a) Kramer Junction, CA (latitude 35.03°N). (b) Petrolina, Brazil (9.35°S).

with time). From the solution graphed in Figs. 6–7, the thermal relaxation time is 6.7 h, which relates exclusively to no-flow conditions.

### 3.5. Correlations for system performance

Correlations are often sought between the monthly electricity delivery $P_e$ and solar input variables. Prior studies often looked for a linear relation with the monthly-average normal beam irradiance $I_{bn}$, but found considerable scatter. The reason is that a given value of daily and monthly-averaged $I_{bn}$ can be realized via distinct unrelated combinations of solar geometry and atmospheric conditions. The physics of the problem indicates that a far better relationship should exist with $Q_{abs}$. The analytic estimates confirm that this is indeed the case, as shown in Fig. 8.

### 3.6. Incidence-angle-modifier effects

The energetic advantage of installing such solar concentrators at lower latitudes is largely reflected in the heightened incidence angle modifier, with a far less acute seasonal dependence at low latitudes. This point is highlighted in Fig. 9, where hourly $K(\theta)$ values are plotted for the solstices and equinoxes. Field measurements show that the annual-average normal beam irradiance is 80% higher in Kramer Junction [33] than in Petrolina [32]. However, the annual-average electricity production is only 56% higher, in large part due to the higher (energy-weighted) $K(\theta)$ for the same solar collectors in Petrolina, complemented by a higher annual-average $\cos(\theta)$. There is also the fringe benefit of a far less pronounced time-of-day and seasonal dependence of power generation at lower latitudes, which means a smaller difference between peak and average power production.

## 4. Conclusions

Analytic modeling not only simplifies the evaluation of the performance of solar thermal power plants, but also provides a clear physical picture of how component and system behavior should vary with key variables such as collector optical and thermal properties, turbine characteristics, and solar beam input. Adopting previously published analytic formulae for turbine performance, and deriving expressions for collector behavior, we have presented a modeling capability for collector and system performance. Straightforward summation of those results over time yields monthly and yearly performance.

In addition, the impact of overnight cool-down, with a collector relaxation time of 6.7 h under no-flow conditions, has been evaluated, and shown to constitute a small but non-negligible fraction of the total energy balance.

The predictions of the analytic modeling were compared against the limited data base for field measurements of the monthly and yearly solar thermal and turbine power delivery from large-scale solar thermal power plants at a mid-latitude location in southern California, with favorable agreement. A theory-vs-experiment comparison was also possible on an hour-by-hour basis, based on the single day for which a complete data was published, with reasonable agreement. Armed with such partial validation, we applied the analytic modeling to performance predictions for an analogous solar thermal power plant planned for a low-latitude site in northeast Brazil.

One aspect of this has been evaluating the tradeoffs at low latitude locations stemming from lower solar beam availability versus the significant gains deriving from solar geometry (i.e., an improved averaged cosine of the incidence angle and incidence angle modifier, with the latter benefitting from higher intercept factors and lower Fresnel reflection losses off the glazing of the evacuated-tube receivers).

Since economic scenarios have proven to be ephemeral, whereas the physics of the problem is immutable, we do not venture into analyses of financial viability. Nonetheless, the fact that close to 5 GW of affordable solar thermal power plants of this nature are currently operating would appear to attest to the cost-effectiveness of such systems, and to justify investigations of the objective scientific and engineering aspects of system modeling and design.

Our analytic model permits a rapid and accurate evaluation of how potential modifications in components, system design and location impact energy delivery. The analytic nature of the model provides a physically transparent picture that clearly explains the major trends for the dependence of system power generation on the principal collector, turbine and operating variables. Furthermore, the general character of the formulation allows it to be applied to a variety of solar power systems, in contrast to most available numerical simulation models that are rather focused upon a particular system and can be quite complex.

## Acknowledgments

This research was funded by CAPES (Brazil) Project 88881.067984/2014–01. JMG is grateful to Professors Olga Vilela and Naum Fraidenraich for their hospitality during part of the period of this research.

## References

[1] Teske S, Leung J, Crespo L, Bial M, Dufour E, Richter C. Solar thermal electricity: Global outlook 2016. Brussels, Belgium: European Solar Thermal Electricity Association; 2016.

[2] Price H. A parabolic trough solar power plant simulation model. In: Proc. ASME 2003 International solar energy Conference. Paper No. ISEC2003-44241. Pp. 665–673. Kohala Coast, HI; 2003.
[3] Salgado-Conrado L, Rodriguez-Pulido A, Calderón G. Thermal performance of parabolic trough solar collectors. Renew Sustain Energy Rev 2017;67:1345–59.
[4] DLR. Greenius energy yield calculation Software. August 23, 2016. http://www.dlr.de.
[5] NREL. System advisor model. April 5, 2010. https://sam.nrel.gov/.
[6] Alobaid F, Mertens N, Starkloff R, Lanz T, Heinze T, Epple B. Progress in dynamic simulation of thermal power plants. Prog Energy Combust Sci 2016;59:79–162.
[7] Al-Maliki WAK, Alobaid F, Kez V, Epple B. Modelling and dynamic simulation of a parabolic trough power plant. J Process Control 2016;39:123–38.
[8] Forristall R. Heat transfer analysis and modeling of a parabolic trough solar receiver implemented in engineering equation solver. In: NREL Technical report NREL/TP-550–34169. NREL, Golden, CO; Oct. 2003.
[9] Suojanen S, Hakkarainen E, Tähtinen M, Sihvonen T. Modeling and analysis of process configurations for hybrid concentrated solar power and conventional steam plants. Energy Convers Manag 2017;134:327–39.
[10] Barcia LA, Menéndez RP, Esteban JAM, Prieto MAJ, Ramos JAM, de Cos Juez FJ, et al. Dynamic modeling of the solar field in parabolic trough solar power plants. Energies 2015;8:13361–77.
[11] Fontalvo A, Garci J, Sanjuan M, Padilla RV. Automatic control strategies for hybrid solar-fossil fuel power plants. Renew Energy 2014;62:424–31.
[12] Menéndez RP, Martínez JA, Prieto MJ, Barcia LA, Sánchez JMM. A novel modeling of molten-salt heat storage systems in thermal solar power plants. Energies 2014;7:6721–40.
[13] Desai NB, Bandyopadhyay S. Optimization of concentrating solar thermal power plant based on parabolic trough collector. J Clean Prod 2015;89:262–71.
[14] De Luca F, Ferraro V, Marinelli V. On the performance of CSP oil-cooled plants, with and without heat storage in tanks of molten salts. Energy 2015;83:230–9.
[15] Desai NB, Kedare SB, Bandyopadhyay S. Optimization of design radiation for concentrating solar thermal power plants without storage. Sol Energy 2014;107:98–112.
[16] Boukelia TE, Arslan O, Mecibah MS. Potential assessment of a parabolic trough solar thermal power plant considering hourly analysis: ANN-based approach. Renew Energy 2017;105:324–33.
[17] NREL concentrating solar power projects. Solar electric generating station VI. October 1, 2015. https://www.nrel.gov/csp/solarpaces/project_detail.cfm/projectID=33.
[18] Rolim M, Fraidenraich N, Tiba C. Analytic modeling of a solar power plant with parabolic linear collectors. Sol Energy 2009;83:126–33.
[19] Rabl A. Active solar collectors and their applications. New York: Oxford University Press; 1985.
[20] Fraidenraich N, Oliveira C, Vieira da Cunha AF, Gordon JM, Vilela OC. Analytical modeling of direct steam generation solar power plants. Sol Energy 2013;98:511–22.
[21] Incropera FP, DeWitt DP. Fundamentals of heat and mass transfer. fourth ed. NY: Wiley; 1996.
[22] Technical Bulletin 7239115B, Therminol® VP-1, vapor phase/liquid phase heat transfer fluid, 12°C to 400°C. St. Louis, MO: Solutia Inc.; 1999.
[23] Dudley VE, Kolb GJ, Mahoney AR, Mancini TR, Matthews CW, Sloan M, et al. Test results SEGS LS-2 solar collector. Sandia National Laboratories technical report SAND94-1884; Dec. 1994. www.nrel.gov/csp/troughnet/pdfs/segs_ls2_solar_collector.pdf.
[24] Patnode AM. Simulation and performance evaluation of parabolic trough solar power plants. MSc thesis. Mechanical Engineering Department, University of Wisconsin-Madison; 2006.
[25] Fraidenraich N, Gordon JM, Fernandes de Lima RC. Improved solutions for temperature and thermal power delivery profiles in linear solar collectors. Sol Energy 1997;61:141–5.
[26] Hirsch T, Schenk H, Schmidt N, Meyer R. Dynamics of oil-based parabolic trough plants - impact of transient behaviour on energy yields. In: Proc. 16th solar PACES Conference, Perpignan, France; 2010.
[27] Moser M. Combined electricity and water production based on solar energy. PhD Thesis. Germany: Faculty of Energy and Biotechnology, University of Stuttgart; 2014. http://elib.uni-stuttgart.de/bitstream/11682/2382/1/Moser_M._2014_Diss_Combined_Electricity_And_Water_Production_Based_On_Solar_Energy.pdf.
[28] Cable R. Solar trough generation: the California experience. Washington, DC: American Solar Energy Society Forum; June 2001. http://infohouse.p2ric.org/ref/46/45464.pdf.
[29] Van Wylen GJ, Sonntag RE, Borgnakke C. Fundamentals of classical thermodynamics. fourth ed. New York: Wiley; 1994.
[30] Vieira da Cunha AF, Fraidenraich N, Vilela OC. Endoreversible and conventional analysis of a Rankine power cycle: comparison with Rankine cycle. In: Proc. COBEM 2011-21st International Congress of mechanical engineering; 2011. p. 10–20. Natal, RN, Brazil.
[31] Stuetzle T, Blair N, Mitchell JW, Beckman WA. Automatic control of a 30 MWe SEGS VI parabolic trough plant. Sol Energy 2004;76:187–93.
[32] National Institute for Space Research. INPE SONDA environmental data base. Brazil: São José dos Campos; July 12, 2016. sonda.ccst.inpe.br/basedados/petrolina.html.
[33] NREL solar radiation archives. Feb. 23, 2017. www.nrel.gov/solar.